CubeSat Camera: A Low Cost Imaging System for CubeSat Platforms

Elise Allthorpe-Mullis[1)], William Brzozowski[2)], William Easdown[1)], Dylan Feore[1)], William Grainger[1)], Steve Greenland[2)], Max Hodgkins[1)], Maria Milanova[2)], Steve Payne[1)], David Pearson[2)], Charlotte Rowan[3)] and Stephen Todd[2)]

1) RAL Space, STFC, Harwell Campus, Didcot, United Kingdom
2) UK Astronomy Technology Centre, STFC, Edinburgh, United Kingdom
3) Business and Innovations Department, STFC, Harwell Campus, Didcot, United Kingdom

(Received 25th May 2018)

RAL Space and UK Astronomy Technology Centre have a wealth of knowledge in developing bespoke imaging systems for various applications, from astronomy to earth observation. Interest in the capabilities of small satellites led to the CubeSat Camera (CCAM); a proof of concept design for a modular, low cost imaging system, compatible with a CubeSat platform. CCAM's imaging system consists of a Cassegrain-style telescope with a field correcting lens and CMOS detector, all within a 1.5U volume. CCAM's telescope and detector are two separate modules, which allows each to be tested and used separately. By having the imaging system consist of modular components, CCAM can be modified according to specific missions. For example, imaging in the near-infrared can be accomplished by removing the NIR blocking filter and changing the detector module to a monochrome detector. CCAM is designed to be diffraction limited – or near diffraction limited – across visible and near-infrared wavebands and continues this performance across a 400km-700km orbital height range. Radiation hardening for Low Earth Orbit allows for a 1-2yr lifetime. Many opto-mechanical design points are considered to reliably achieve high image performance in such a small volume. For example, the design of light baffles to eliminate stray light and the optical mounting mechanisms to maintain tight tolerances whilst not vignetting science light. The CCAM system is designed to be optically aligned within its 1.5U, and is therefore independent of the rest of the CubeSat platform. The electronics will be laid out on a double-sided PCB. A custom mount will attach the PCB to the camera. The CMOS sensor takes ~500µs exposures that can be stitched into a swath (at the ground station). Data are fed to the customer's On-Board Computer via 16 pairs of LVDS lines at 28Mbps. The electronics require a 3.3V, 3A power supply. The supply is subdivided into 5 voltage rails (1.5V, 2.1V, 2.5V, 3V, 3.3V) where no one rail will exceed 2A. CCAM aims to achieve 5m ground sampling distance across the visible wavebands at a 400km orbit. This is a high resolution for a small satellite, and enables CCAM to be utilised in a broad range of Earth Observation applications. However, the applications are not limited to EO. This technology could be used to observe other solar system bodies. For example, the geological activity of Europa, the meteoroid environment of the Moon, or the weather systems and landscapes of Mars.

Key words: CubeSat, Imaging System, Camera

Nomenclature

AR	Anti-reflection
CCAM	CubeSat Camera
CSK	CubeSat Kit
EO	Earth Observation
FEA	Finite Element Analysis
FPU	Focal Plane Unit
GEVS	General Environmental Verification Standard
GIQE	General Image Quality Equation
GRD	Ground Resolvable Distance
GSD	Ground Sampling Distance
LEO	Low Earth Orbit
MTF	Modulation Transfer Function
NIIRS	National Image Interpretability Rating Scale
NIR	Near Infrared
OBC	On Board Computer
OT	Optical Telescope
RER	Relative Edge Response
RMS	Root Mean Squared
SNR	Signal to Noise Ratio

1. Introduction

Since their initial proposition by Twiggs et al. [1] and first flights in 2003, the capability of CubeSat systems has been steadily increasing [2]. Initially used as hands-on tools in universities, CubeSats now offer a cost-effective enabler for new mission services and architectures. A 2018 market forecast estimates 2,600 new nano/micro satellites will be launched in the next five years [3]. In the Earth Observation (EO) domain Planet lead the way, offering sub-4 m resolution imagery from a constellation of CubeSat and small satellite systems with a monthly cloud-free base map [4].

This paper will outline the design, performance and potential applications of the CubeSat Camera (CCAM); a modular, low cost imaging system, compatible with the CubeSat platform. CubeSat Camera is a proof of concept design being developed by RAL Space and the UK Astronomy Technology Centre. The system advances the capacity of these organisations to deliver off-the-shelf or bespoke imaging solutions into the CubeSat market, able to harness heritage and expertise gained in high performance space and ground-based instruments such as RALCam-3 on the International Space Station (ISS) [5], and the infra-red science instrument MIRI on JWST [6].

2. System Overview

The CCAM Module consists of two modular and exchangeable modules, the Optical Telescope (OT) and the Focal Plane Unit (FPU). A model of the system integrated into a CubeSat structure can be seen in *Figure 1*.

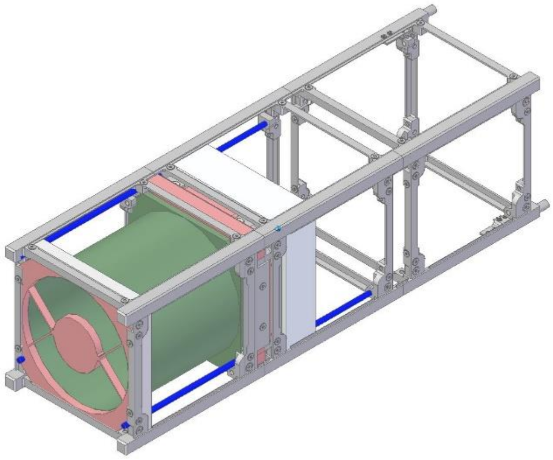

Figure 1: A CAD model of the CCAM Imaging System, made up of the FPU and OT units

The interface between the two modules is largely defined in terms of mechanical alignment and optical properties. *Figure **1*** provides a functional breakdown of this system architecture in terms of the elements and the engineering disciplines to which they belong. As an iterative design to establish a realistic design point rapidly, not all functionalities particularly within the FPU have been targeted in this first iteration.

In addition to the internal interface between the FPU and the OT, interfaces to the CubeSat bus have to be considered, and in particular for CCAM:

- command and data handling, conforming to typical CubeSat OBC and software system,
- electrical interfaces including backwards compatibility with (CubeSat Kit) CSK PC104 and harnessing,
- mechanical interfacing to a range of off-the-shelf CubeSat structures,
- thermal limits and opportunities for dumping excess heat from the payload system,
- ADCS stability requirements necessary to achieve the baseline performance.

3. CCAM uses and market

CCAM is an off-the-shelf imaging system designed for EO applications, with potential for interplanetary use. It has been designed to consist of modular components to allow flexibility and integration of the camera into a wide range of different missions. This gives customers a fast and cheap option to launch their mission.

The global commercial satellite imaging market is a large growth area, with increasing demand for high resolution imagery. The market was valued at US $1.6Bn in 2014, and is projected to reach US$3.5Bn by 2024 [7]. The use of CubeSats in satellite imaging, particularly EO, is rapidly increasing with the small satellite EO market value expected to be US$347M over the next six years [8]. Sectors making use of EO satellite imagery include defence and security, insurance, disaster monitoring, agriculture, civil engineering and energy, as well as government use.

Image providers, such as Planet [4], who currently operate a constellation of CubeSats to provide high temporal resolution EO images, dominate the CubeSat imaging market. Options for commercial off-the-shelf imaging systems for others to purchase and integrate into a CubeSat are limited and mostly offer low spatial resolution, making them unfit for many EO applications.

In addition to EO, CCAM has potential for interplanetary use, with possible applications including geological activity monitoring of Europa and other solar system bodies, observation of the meteoroid environment of the Moon, or the weather systems and landscapes of Mars.

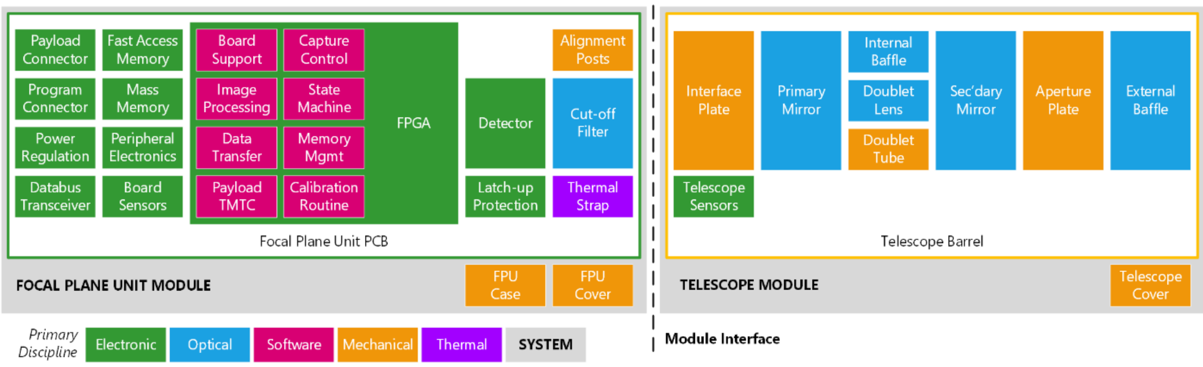

Figure 2: System decomposition into functional elements of the FPU and OT units

4. Design Drivers

The design drivers for CCAM reflect the product driven approach adopted for the development. The work emphasises the use, wherever feasible, of off-the-shelf components with consideration to their suitability to the LEO (and launch) environments in order to reach a lower price point. A range of off-the-shelf CubeSat buses and interfaces have been considered to ensure potential compatibility. As a result, the 1.5 U module is defined for the payload of up to 1.5 kg in mass in line with the interfaces noted above. The baseline uses a single aperture optical telescope system mounted in the long axis of the CubeSat. The use of a RGGB Bayer pattern off-the-shelf CMOS detector FPGA FPU design allows the reuse of existing experience and electronics within the team. Although this limits the maximum performance achievable within the baseline, it provides a route to enhance capability through either/or the option for monochrome with custom-filters, and integration techniques within the FPGA.

5. Baseline Performance

Three drivers dominate the image quality available from a satellite system, the Ground Sampling Distance (GSD), Modulation Transfer Function (MTF), and Signal to Noise Ratio (SNR). Combined with appropriate post-processing, these metrics inform the quality in terms of the ability to process and interpret the image captured for a given application. The National Image Interpretability Rating Scale (NIIRS) provides a subjective rating of an image interpretability [9], initially developed for drone operators. In typical high performance systems, GSD is the most significant driver, contributing > 70% in terms of overall interpretability [10].

For the CCAM project an NIIRS of at least 2 is targeted, a sample image depicted in *Figure 3*. A NIIRS level 2 rated system should allow feasible detections, through human interpretation, covering the following:

- identify large (i.e., greater than 160 acre) centre-pivot irrigated fields during the growing season,
- detect large buildings (e.g., hospitals, factories),
- identify road patterns, like clover leafs, on major highway systems,
- detect ice-breaker tracks,
- detect the wake from a large (e.g., greater than ca. 91m) ship.

Figure 3 - Reference image performance for a NIIRS level 2 rated system [9].

Although the NIIRS was established as a human evaluated scale; subsequently a five-parameter General Image Quality Equation (GIQE) has been defined based on sampled coefficients and is now on its fifth release [11]. The GIQE also aligns the NIIRS with the minimum Ground Resolvable Distance (GRD). The five input parameters into the GIQE are, Ground Sampling Distance (GSD), Signal to Noise Ratio

(SNR), Relative Edge Response (RER), Convolver Gain (G), and Edge Overshoot (H).

The GSD is a function of the optical design and orbit geometry, constrained by the physical limits of the module and the detector pixel size (noting the impact of the Bayer pattern). Based on CubeSat state of the art, a GSD requirement of 5 m is proposed across LEO altitudes [12].

The SNR is again constrained by the physical design and the orbit dynamics, taken before any post-processing, although will vary dependent upon what constitutes signal and noise in the target application. Above a threshold, the SNR will improve the uncertainty in the measurement following radiometric calibration. For terrain monitoring, NASA specifications for LandSat-like applications 100:1 would be a goal, limiting the uncertainty to < 3%; however for CCAM a firm requirement of greater than 20:1 is mandated, based on comparable CubeSat systems and reasonable performance [13].

The MTF may be considered as a product of the optical, detector, and platform MTFs. In the context of an off-the-shelf imager payload, the first two MTF products may therefore be associated with requirements on the Payload to achieve a given image quality. The latter associated dominated by any ADCS, timing and any thermal effects will be a constraint upon the integrator to ensure that the platform does not exceed limits for payload performance. The final three parameters RER, G and H and all practical metrics of the system Modulation Transfer Function (MTF) usually taken after image post-processing, with the most significance typically placed on the RER. The RER is a measure of the pixel to pixel sharpness and will be impacted by the inclusion of the Bayer patterned detector and subsequent interpolation performed. As post-processing cannot be considered in this context, only the RER is specified in the typical range of imaging systems: 0.5-0.6.

6. Optics Module

The main constraints on the optics are the volume, GSD, altitude, pixel size and wavelength range. The CMOS detector determined the pixel size as 5.5µm and the detectable wavelength range as 400nm-900nm. The optics volume was limited to 1UX1UX1.2U, determined by the 3U CubeSat size. The altitude was determined by LEO boundaries and launch limitations e.g. an ISS launch. The required GSD of 5m and the altitude and pixel size constraints determined that a focal length of 520mm was needed.

Reflective and refractive optical designs were both considered for CCAM. However, the volume constraints and required focal length determined CCAM to be a reflective design, as for a refractive design it is not feasible to fit a 520mm focal length into a 120mm length optics module. The resultant optical design is shown in *Figure 4*.

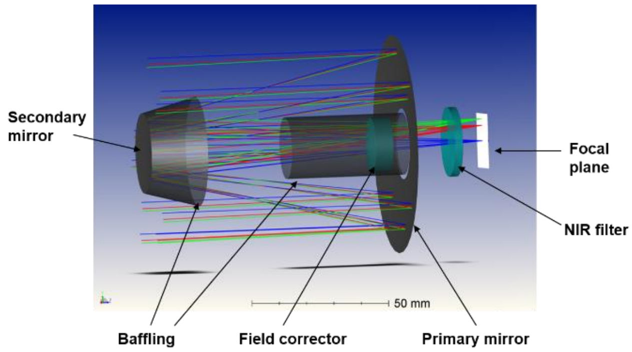

Figure 4 – Optical layout for CCAM

CCAM has an AR-coated doublet field correcting lens between the secondary and the detector module. This lens flattens the field and reduces aberrations. The radiation environment in LEO has been considered by using radiation-hardened glass for the field corrector. A NIR blocking filter is also included in the design for accurate colour imaging as recommended by the sensor manufacturer. CCAM is optimised to continue its good performance into the NIR, giving the option of removing this NIR filter and using a monochrome CMOS sensor for NIR imaging.

Stray light is a significant problem for EO, especially for a reflective design. *Figure 4* shows the designed light baffles that eliminate stray light whilst minimising vignetting of science light. The central tube is dual purpose as it acts as a light baffle as well as a mounting point for the field corrector.

CCAM's optical module gives diffraction limited performance over the visible and NIR wavelength range, as shown in *Figure 5*. The RMS of the spot radius seen at the detector is smaller than the diffraction limit, hence optical aberrations are negligible. *Figure 5* represents the nominal system, but given mechanical tolerances this performance will degrade. However, CCAM is designed to allow high precision adjustment of the most sensitive degrees of freedom of the optical components. This enables an optical alignment process that can correct for mechanical tolerances and achieve CCAM's diffraction limited performance.

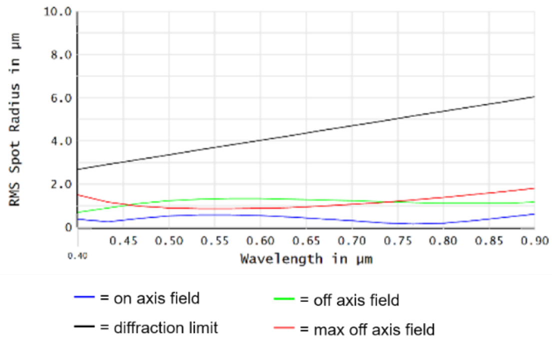

Figure 5 – RMS spot radius vs. wavelength

The optical performance is sensitive to the thermal expansions and contractions of the CubeSat body. Considering the LEO thermal environment, an operational temperature range of -20ºC < T < 60ºC is to be expected. A passive thermal control mechanism will compensate for any thermal expansion/contraction and allow the optics module to continue its performance across the temperature range.

7. Optomechanical Design

The optical telescope (OT) module takes up 1.2 U of CCAM's overall 1.5 U volume and is physically connected to the FPU module using a 3-point kinematic mount to ensure preservation of optical alignment between both units. This connection is accomplished using a dedicated interface surface which detaches from the back of the primary mirror mount but is reinforced to ensure structural stability.

The telescope unit has been designed so that it can be integrated into various CubeSat structures and the integration of solar panels has also been accounted for in the design.

Design decisions have been driven by the restricted space available, mitigating the effects of thermal changes and launch vibration loads on the structure as well as blocking off stray light and providing adjustable optical alignment capabilities. The module consists of separate mounts for the primary and secondary mirror, and a lens tube mounting design for the field corrector as well as light baffles. The module is provided with different mounting features depending on the outside structure chosen by the customer.

Both the primary and secondary mirror mounts employ kinematic designs to allow for repeatable sub-millimetre precision alignment. The secondary mirror mount is held in place by a spider leg configuration so as not to obstruct the optical path. Axial and radial passive thermal compensation features are also incorporated in the design which maintain the optical alignment under all operating conditions. Vibration dampeners are employed surrounding the optics to mitigate launch load vibration effects. FEA analysis will be performed to test the structure integrity under various launch conditions.

The mechanical design has been outlined in *Figure **6***.

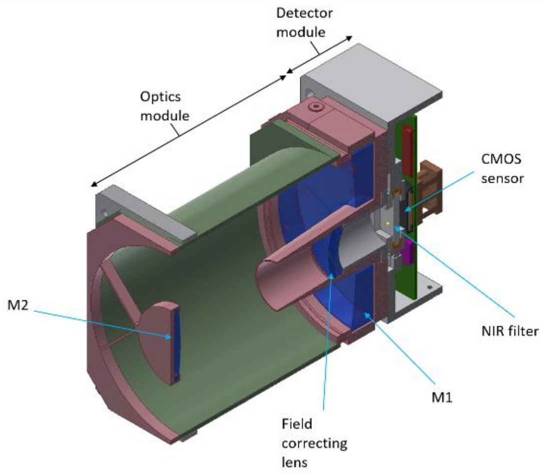

Figure 6: Mechanical design outline. From left to right: secondary mirror mount, lens barrel, primary mirror mount.

Moreover, alignment features have been accounted for in the design process. The features most sensitive to slight misalignment are tip, tilt and axial position of the two mirror segments. The back plate for the primary mirror has been chosen as the reference optical element, which means that all optical components need to be adjustable in 5 degrees of freedom to match this. The primary and secondary mirror mount design addresses this by shims available in tip, tilt and on axis location and decentration. These shims are cleverly incorporated into existing design features so as not to add extra complexity and weight to the structure. The field corrector, which sits in a lens cell-type configuration, will be secured in place by an insert which can also act as a shim for optical adjustments.

8. Detector Module

The electronics components of CCAM are all contained within a single PCB, which we have called the Focal Plane Unit (FPU). In the centre of this board is the 2048x2048 pixel CMOS sensor, with the FPGA that is used for controlling the module sitting adjacent to the sensor.

The FPU's electronics have been designed with a CubeSat's stringent power requirements in mind. The FPU will utilise the 3V3 and unregulated 6V lines commonly found on CubeSats, with all other voltages that are required by the electronics being generated internally by low noise linear regulators. No more than 2A will be drawn from a single line and overall maximum power draw will be around 6W. This power requirement should be sufficiently low to enable extended operation during sunlit orbit phases.

CCAM operations have been optimised both in terms of power usage and image quality. Low active current draw will be complemented by a selection of power modes. These will turn off particular components to put the camera into standby or quiescent only modes, greatly reducing the power requirement when the camera is not being used for imaging. Image blur is minimised through use of 500µs exposures, with an overall frame rate of 0.5fps. FPGA RAM is used as a line buffer to allow for any small delays in OBC processing of image data.

Design considerations include a thermal strap leading away from the CMOS sensor to dissipate its heat to the chassis, and low electrical noise through the use of linear rather than switch mode regulators. These will maximise the usability and lifetime of the FPU.

9. Mechanical Design of Detector Module

The FPU serves to mechanically connect the electronics to optics module. It also unites the electronics, thermal strap and cut-off filter into one module. The modularity of the design facilitates ease of assembly and potential use with other systems. The FPU is 0.3 U thick and is located behind the Optics module; at the centre of a 3U CubeSat assembly. An image of the FPU can be seen in *Figure **7***.

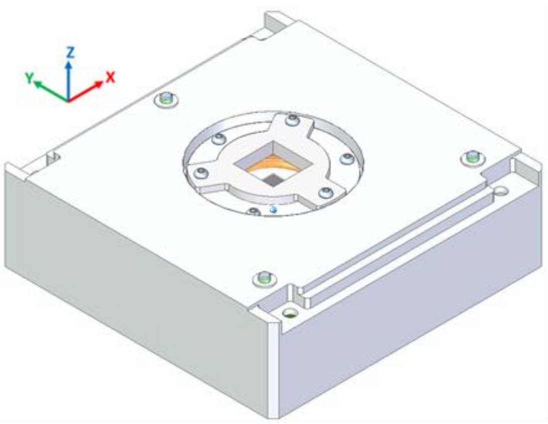

Figure 7: Top isometric view of the FPU assembly

9.1. Design Overview

There are many design constraints resulting from other areas of design. These constraints are: radiation protection, optical alignment, accessibility and CubeSat standard.

The foundation of the FPU design is the encapsulating box, for radiation protection and blocking of incident light. Each electronic component has a given radiation hardness, if this threshold is reached then its desired function is diminished. The encapsulating box is made up of three main components: overall box, filter mount and back cover. The back cover provides an interface for customer systems and facilities accessibility to the FPU interior.

Alignment of the detector and the optics is another integral aspect of the FPU design. For this reason, the FPU is mounted directly to the Optics module and not to the CubeSat structure. Assembling the CCAM system separately ensures alignment, avoiding misalignment due to less stringent CubeSat structure tolerances. The FPU is aligned to the Optics through a three point kinematic mount - three bolts between the FPU and interface plate. Tight tolerances are required to achieve proper alignment of the detector. The most important degrees of freedom, with the tightest tolerances, are Z distance and rotation about X and Y.

The cut-off filter is supported between the detector and optics. The filter mount is removable so that different filters can be used. The top side of the filter mount can be seen in *Figure **7***; bolts fix the filter mount to the FPU box and facilitate the removability. A cover is placed over the sensor until assembly with the optics. The cover can be removed by temporarily taking the filter mount out, instead of disturbing the detector alignment by removing the PCB.

The PC104 CubeSat standard is an important feature for system compatibility. PC104 rods connect CCAM to the CubeSat structure. To maintain alignment within CCAM the PC104 rods pass through but do not make contact with the FPU. The PC104 holes are located in the 4 corners of the FPU, shown in *Figure 7*.

A thermal strap connects from the back of the sensor and through the PCB, providing a mechanical interface for thermal control by the customer. The thermal strap is discussed more in section 9.3.

9.2. Analysis

The vibrations experienced by a sub 22.7 kg payload during launch are shown in *Figure **8***; the overall acceleration experienced is 14.1 G_{rms}, on the FPU to ensure it is designed to withstand and protect the contents for operation.

Frequency (Hz)	ASD Level (g^2/Hz)	
	Qualification	Acceptance
20	0.026	0.013
20-50	+6 dB/oct	+6 dB/oct
50-800	0.16	0.08
800-2000	-6 dB/oct	-6 dB/oct
2000	0.026	0.013
Overall	14.1 G_{rms}	10.0 G_{rms}

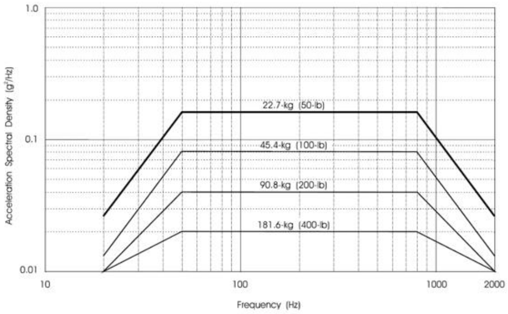

Figure 8: NASA GEVS Generalised random vibration test levels for launch – sub 22.7 kg payload [14]

During operation in LEO the CCAM system will experience environmental radiation, which it needs to withstand, in particular trapped particle radiation in the radiation belts. A possible radiation environment, for a Sun Synchronous orbit, is illustrated in *Figure 9* and *Figure 10*. This example uses the solar maximum model version and displays electron and proton energies over 1 day of CCAM operation.

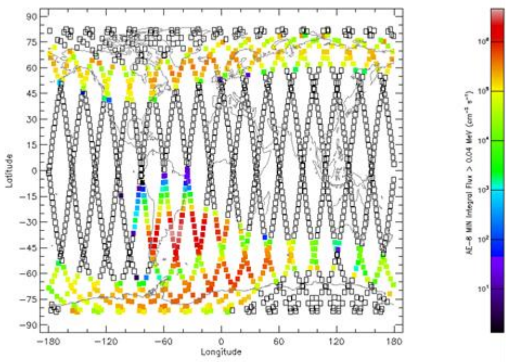

Figure 9: Trapped Electron Flux displayed on a world map for a Sun Synchronous orbit at 574km and ascending node of 12.

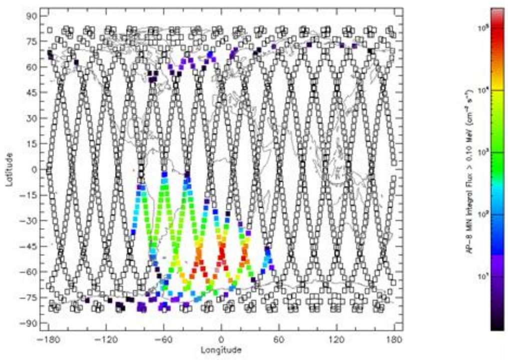

Figure 10: Trapped Proton Flux displayed on a world map for a Sun Synchronous orbit at 574km and ascending node of 12.

To ensure the electronic components within the FPU are protected from the radiation environment, the FPU design includes shielding as shown in *Figure 7*. For the above 2mm Aluminium shielding, the illustrated Sun Synchronous orbit and a lifetime of 2 years, the ionising dose on the detector is 3 krad.

9.3. Thermal Considerations

The instrument utilises a passive thermal control system that aims to improve conductive links and radiative heat exchange where necessary.

The FPU consists of a PCB with a CMOS sensor, voltage regulators and an FPGA. The thermal control of the CMOS sensor is particularly critical as the dark noise performance degrades at temperatures above 25°. The sensor has an internal power dissipation as well as an incident flux from the optical assembly increasing the total heat load on the sensor. To achieve this temperature performance a passive control system consisting of a thermal adhesive and copper thermal strap has been employed. The thermal adhesive bonds the thermal strap to the back of the sensor. The thermal strap then provides an interface for the customer to control the temperature of the sensor. To ensure the temperature performance of the sensor the customer is required to dissipate the resultant heat flux and maintain the interface at a given temperature below 25°C. The voltage regulators and FPGA also dissipate a substantial amount of power. The voltage regulators have been stuck to the PCB using thermal adhesives when necessary. The FPGA utilises its solder pattern for conduction; an additional thermal strap can be applied if required. A conformance coating can also be applied to the PCB and its components, excluding the sensor, to improve radiative heat exchange to the housing. The PCB itself will dissipate heat to the housing conductively through three mounts and radiatively through the high emissivity coating.

The thermal design of the optics assembly is discussed in Section 7. The FPU housing and sensor mount is made from the same grade of aluminium as the optics assembly. Therefore, the coefficient of thermal expansion is similar for both assemblies; minimising possible misalignment due to temperature variations across the orbit.

The overall optical surface properties of both the optics and sensor assemblies can be tailored to maintain operating conditions given the customer's CubeSat outer panelling.

10. System Signal to Noise Performance

Table 1 - Baseline signal to noise performance

SNR PERFORMANCE: BASELINE		R			G			B			
		Typical	High	Cloud	Typical	High	Cloud	Typical	High	Cloud	Units
Signal											
Detector area	A	3.03E-11	3.03E-11	3.03E-11	3.03E-11	3.03E-11	3.03E-11	3.03E-11	3.03E-11	3.03E-11	m2
Centre wavelength	lambda	630	630	630	540	540	540	470	470	470	nm
Bandwidth	BW	150	150	150	150	150	150	150	150	150	nm
Spectral radiance in band	Ltyp	40	190	602	30	194	602	22	150	602	W.sr-1.m-2.um-1
Optical transmittance	tau	0.60	0.60	0.60	0.60	0.60	0.60	0.60	0.60	0.60	
Quantum efficiency over bandwidth	QE	0.4	0.4	0.4	0.4	0.4	0.4	0.4	0.4	0.4	
Exposure time	t	678	678	678	678	678	678	678	678	678	us
f-number	f#	5.5	5.5	5.5	5.5	5.5	5.5	5.5	5.5	5.5	
Pixel solid angle	rho	0.026	0.026	0.026	0.026	0.026	0.026	0.026	0.026	0.026	sr
Photons per watt	nph	3.17E+18	3.17E+18	3.17E+18	2.72E+18	2.72E+18	2.72E+18	2.37E+18	2.37E+18	2.37E+18	ph.W-1
Signal in exposure	S	2431	11545	36580	1563	10104	31354	997	6800	27290	e-
Well capacity	nevmax	13500	13500	13500	13500	13500	13500	13500	13500	13500	e-
Saturation	S	18%	86%	271%	12%	75%	232%	7%	50%	202%	
TOTAL SIGNAL	**Stotal**	**2431**	**11545**	**13500**	**1563**	**10104**	**13500**	**997**	**6800**	**13500**	**e-**
Noise											
Shot noise	Ns	49.3	107.4	191.3	39.5	100.5	177.1	31.6	82.5	165.2	e-
Readout	Nr	13.0	13.0	13.0	13.0	13.0	13.0	13.0	13.0	13.0	e-
Dark current noise	Ndc	0.1	0.1	0.1	0.1	0.1	0.1	0.1	0.1	0.1	e-
Quantisation noise	Nq	13	13	13	13	13	13	13	13	13	e-
Atmospheric scatter	Ns	15.6	34.0	60.5	12.5	31.8	56.0	10.0	26.1	52.2	e-
TOTAL NOISE	**Ntotal**	**55**	**115**	**202**	**45**	**108**	**187**	**38**	**89**	**175**	**e-**
RESULTANT SNR	**SNR**	**33**	**75**	**50**	**26**	**70**	**54**	**20**	**57**	**58**	

SNR performance will vary with wavelength due to variations in radiance and transmissivity of the optics. The CMOS sensor has a maximum well capacity of 13500 e^-, which will limit the dynamic range and make a push array mode of operation preferable to point and stare. As a result, and with single exposures over a single 5 m GSD pixel driving a very short exposure time (~700 us) to avoid blur, the maximum signal photon count at the aperture is limited. In the future, this may be overcome by oversampling the detector over the pixel flight time, inserting beamsplitting gratings/prism optics feeding multiple detectors, or using deployable apertures.

The baseline SNR performance in the three R, G, B bands is given in *Table 1*. Optical and electronic noise sources are considered within the budget. Given the short exposure time this will be dominated by Shot and Readout noise: the assumption fixed pattern and glint noise sources may be made negligible through calibration and pointing offsets respectively.

It may be observed that the cloud case causes saturation in the detector. Due to the use of CMOS technology, blooming and smearing will not be an issue in CCAM and can be ignored. Typically, on saturation the detector will readout white pixels, and excess charged will be drained, meaning no impact on subsequent exposures. Provided an adequate margin is maintained over the high luminance case, saturation due to cloud can therefore be distinguished in post-processing and the dynamic range of the detector for useful imaging maximised. The Black Sun effect, where these white pixels are inverted due to extremely bright light, may be mitigated by ensuring that the time between the start of exposure and readout – and subsequent reset – is minimised.

11. Conclusions

Projected applications for CCAM are wide-ranging due to the flexibility in the design and potential for future developments. CCAM can be utilised in a wide range of EO applications and has been designed with this market in mind. CCAM will be suitable for other applications and this potential will be explored in future developments. It is anticipated that CCAM could be of value for terrestrial applications, such as nuclear waste monitoring, as well as interplanetary applications, such as the monitoring of weather systems and landscapes of Mars.

The modular design offers a baseline to consider performance enhancements, such as use of deployable optics to achieve sub-1 m GSD, and detector options to offer multispectral or higher SNR solutions. The use of oversampling and in-firmware time delayed integration techniques may allow an SNR of 100 to be reached. Next steps will consider: (a) the qualification and characterisation of off-the-shelf parts selected in a LEO environment; (b) engagement with lead-in potential customers to refine the performance specification against a specific application requirement; (c) prototyping the manufacture, assembly, integration and test processes for CubeSat systems with existing facilities across STFC; and (d) consideration as to the image processing chain (in particular post-processing algorithms) supported by the operations and performance of this class of imager.

Acknowledgements

The authors gratefully acknowledge funding from the STFC Proof of Concept fund.

References

[1] H. Heidt, P.-S. J, A. Moore, S. Nakasuka and R. Twiggs, "CubeSat: A new generation of picosatellite for education and industry low-cost space experimentation," in *14th USU Conference on Small Satellites, SSC-V-5*, Utah, US, 2000.

[2] M. Swartwout, "The first one hundred CubeSats: a statiscal look," *Journal of Small Satellites*, vol. 2, no. 2, pp. 213-233, 2013.

[3] B. Doncaster, C. Williams and J. Shulman, "Nano/Microsatellite Market Forecast," SpaceWorks Commercial, Atlanta, 2018.

[4] Planet, "Planet Hompage," [Online]. Available: www.planet.com. [Accessed May 2018].

[5] RAL Space, "Epic spacewalk will put us in the front row for near live video of the Earth," RAL Space, 29 January 2014. [Online]. Available: https://www.ralspace.stfc.ac.uk/Pages/Epic-spacewalk-will-put-us-in--the-front-row-for-near-live-video-of-the-Earth.aspx. [Accessed May 2018].

[6] G. Wright, G. Reike, P. Barella, T. Boeker, L. Colina, E. van Dishoeck, P. Driggers, G. Goodson, T. Greene, A. Heske, T. Henning, P. Lagage, M. Meixner, H. Norgaard-Nielsen, G. Olofsson, T. Ray, M. Ressler, J. Thatcher, C. Waelkens, D. Wright and A. Zehnder, "Design and development of MIRI, the mid-IR instrument for JWST," *Proceedings of SPIE Astronomical Insrtrumentation and Telescopes*, vol. 7010, 2008.

[7] Euroconsult, "Satellite-Based Earth Observation: Market Prospects to 2024," Euroconsult, September 2015. [Online]. Available: http://www.euroconsult-ec.com/16_September_2015. [Accessed May 2018].

[8] C. Anderson, C. Brunskill and C. Guillo, "Small is the new Big - White Paper," May 2014. [Online]. Available: https://sa.catapult.org.uk/wp-content/uploads/2016/03/Small-is-the-new-Big.pdf. [Accessed May 2018].

[9] J. Pike, "National Image Interpretability Rating Scales," FAS Intelligence Resource Program, 16 January 1998. [Online]. Available: https://fas.org/irp/imint/niirs.htm. [Accessed April 2018].

[10] A. Ali, F. Eltohamy and G. Sala, "Estimation of NIIRS for high resolution satellite Images using the simplified GIQE," *Journal of Innovative Research in Computer and Communications Engineering*, 2016.

[11] J. Leachtenauer, W. Malila, J. Irvine, L. Colburn and N. Salvaggio, "General Image Quality Equation: GIQE," *Applied Optics*, vol. 36, no. 32, pp. 8322-8328, 1997.

[12] Planet, "Planet Basemaps Product Specification," Planet Labs Inc, 2018.

[13] Planet, "PlanetScope Scenes API," Planet Labs Inc, [Online]. Available: https://www.planet.com/docs/reference/v0/scenes/planetscope/. [Accessed May 2018].

[14] Goddard Space Flight Centre, “General Environmental Verification Standard (GEVS),” 2013. [Online]. Available: https://standards.nasa.gov/standard/gsfc/gsfc-std-7000. [Accessed 30 04 2018].